Phase-locked particle motion in a large-amplitude plasma wave

Gary R. Smith

Lawrence Livermore Laboratory, University of California, Livermore, California 94550

N. R. Pereira

Lawrence Berkeley Laboratory, University of California, Berkeley, California 94720
(Received 20 March 1978)

A plasma wave with an oscillating amplitude and phase occurs in two commonly studied situations, the beam-plasma interaction and the launching of a large-amplitude wave in a Maxwellian plasma. Electron motion in such a wave is either regular or stochastic. Theoretical study shows that regular motion can exhibit a phase-locking effect, which explains the persistence of amplitude oscillations observed in simulations and experiments. An additional ("test") wave of moderate amplitude can prevent phase-locking, causing stochastic motion instead, and thereby destroy the amplitude oscillations. The effects studied are also relevant to the theory of sideband instability.

I. INTRODUCTION

The evolution of a large-amplitude plasma wave has interested a great number of theorists and experimentalists over many years. Two situations have been treated most extensively. The first situation is that of a wave launched in a Maxwellian plasma. Initially, the wave damps, spatially in experiments or temporally in simulations and in most theories. To be specific, here we use the terms appropriate to the temporal (initial-value) problem. If the linear Landau damping rate γ is much less than the bounce frequency ω_b of an electron in the wave, only modest damping occurs, followed by amplitude oscillations.[1] Oscillations of the wave phase[2] are also observed.[3] The second situation studied extensively is the interaction of an electron beam with a plasma. The beam causes growth of a spectrum of waves, the spectrum narrowing until a single wave (the fastest growing) dominates the electron dynamics.[4] Trapping of beam electrons saturates the wave growth, and the wave subsequently exhibits oscillations in its amplitude and phase.

Several theories, directly applicable to the launched-wave situation, have been proposed to treat the amplitude and phase oscillations. The oscillations result from exchanges of momentum and energy between the wave and the resonant electrons[2] and can therefore be calculated if the exact electron trajectories are known. The earliest theories[1,2] used, instead of the exact trajectories, those calculated for a wave *without* amplitude and phase oscillations. A recent attempt to remedy this lack of self-consistency is reported in Ref. 5. The best available simulation results[6] do not agree with the "self-consistent" theories in all respects, however.

The failures of these purely analytical theories are caused by their inaccurate treatment of the trajectories of some electrons, particularly, the barely trapped and barely untrapped ones. (Statements to this effect have appeared previously, for example in Ref. 7). To construct truly self-consistent theories, the resonant-electron trajectories were computed exactly in "semi-simulation" calculations, two for a large-amplitude wave in a Maxwellian plasma[8,9] and two for the beam-plasma system.[4,10]

In this paper we examine the resonant-electron trajectories in more detail than in work by previous authors. We find that in a wave with oscillating amplitude and phase, some electrons undergo "regular" motion, which can be described analytically. This "regular" motion differs from motion in a wave with constant amplitude and phase. In particular, the well-known phase-mixing process is replaced by a phase-locking effect. Other electrons undergo "stochastic" motion, for which a useful analytical description is not known.

Our ideas have enabled us to understand some of the results of a recent laboratory experiment by Dimonte and Malmberg.[11] The goal of this experiment was to learn about physical processes in the beam-plasma interaction that depend on the nonlinear dynamics of beam electrons. Nonlinearities associated with the plasma were eliminated by replacing it with a traveling-wave tube. With this system, Dimonte and Malmberg observed persistent amplitude oscillations (over five of them) after saturation of the wave; previous beam-plasma experiments had shown a rapid decay of the saturated wave and only about two amplitude oscillations. Persistent oscillations were also observed in the semi-simulation in Ref. 4 and in the full simulation[6] of the evolution of a large-amplitude wave in a Maxwellian plasma.

Another interesting observation of Dimonte and Malmberg,[11] similar to observations in other experiments, is that the amplitude oscillations can be destroyed by the addition of a test wave with a frequency different from the frequency of the original large-amplitude wave (called the main wave). We do not treat a third observation of Ref. 11, that amplitude oscillations can be destroyed by increasing the wave damping. To explain this effect it seems necessary, as in Ref. 12, to consider equations for the self-consistent evolution of the wave amplitude and phase. These equations lie outside the scope of our present work.

 0031-9171/78/2112-2253$00.90

Our numerical calculations, which are designed to model beam-plasma experiments (including the Dimonte–Malmberg experiment), yield the following results: A region of phase space exists in which motion is regular. Many beam electrons are located in that region, implying that there exist long-lived bunches of electrons bouncing in the potential troughs of the wave. These bunches, of course, cause the observed amplitude and phase oscillations. A test wave displaces or destroys the region of regular motion, forcing electrons to move stochastically. This stochastic motion causes dispersal of the bunches.

Our results should also aid in understanding the sideband instability, first observed by Wharton *et al.* [13] The extensive literature on this subject has discussed four physical mechanisms leading to growth of sidebands, waves at frequencies ω differing somewhat from the frequency ω_0 of the main wave.

In the first mechanism, linear sidebands[14] are caused by streaming perturbations introduced during the preparation of the plasma. Experimenters can avoid the linear sideband mechanism by using test waves with amplitudes greatly exceeding the noise level.

The second physical mechanism is referred to by the name "quasi-linear." The many papers dealing with this mechanism vary in their details, but the basic idea of the quasi-linear mechanism seems to be the following. During the initial damping of a large-amplitude wave, the Maxwellian distribution present at $t=0$ is distorted in the vicinity of the phase velocity of the main wave. For intermediate values of γ/ω_b, a positive slope appears on the distribution function for $\pi \lesssim \omega_b t \lesssim 2\pi$, causing the wave amplitude to regrow, but not to its initial level. The resulting distribution function (averaged over subsequent bounce periods) has a positive slope at the phase velocities of waves with frequencies ω satisfying $|\omega - \omega_0| \approx \omega_b$. Test waves with these frequencies show oscillations in their growth rates, but have a significant net growth over the length of the experiment. Theoretical workers have tried to calculate the distribution function near the phase velocity of the main-wave using inexact trajectories for the resonant electrons. [15–17] Experimenters have eliminated the uncertainties of these calculations by measuring the averaged distribution function using energy analyzers. [18–20] The dispersion relation calculated in Ref. 19 from the measured distribution function shows impressive agreement with the measured dispersion of test waves, lending strong support to the quasilinear mechanism in these experiments.

The trapped-particle mechanism[21] for sideband growth requires a population of trapped electrons with a small spread in the frequency of bouncing in the potential wells of the main wave. Our results suggest that such a population indeed exists in the Dimonte–Malmberg experiment; the electrons are not located at the bottom of the potential wells, however. Experiments that have studied the sideband instability have used a launched wave whose amplitude varied considerably. Under these conditions the existence of the required population of trapped electrons seems doubtful to us. Reference 22 claims to have confirmed the trapped-particle mechanism by using a localized perturbing wave to detrap electrons; but, such a wave also affects untrapped electrons, smoothing the distortions in the distribution function that cause sidebands to grow in the quasi-linear mechanism. The appearance of both upper and lower sidebands, initially taken as evidence for the trapped-particle mechanism, [21] can be explained instead by the fourth physical mechanism, passive four-wave coupling. [23]

In Sec. II we discuss a relatively simple dynamical system with motion similar to that encountered in the problem of beam-plasma interaction. Section III gives the potential we use to model a wave with oscillating amplitude and phase. Parameters appropriate to the beam-plasma problem are chosen. Section IV discusses our particle-trajectory calculations, which show a region of regular motion. We find that many beam particles lie in or near this region. In Sec. V we investigate the effect of a test wave on the regular motion. The Appendix uses properties of elliptic integrals and functions to derive some formulae needed in Sec. II.

II. REGULAR AND STOCHASTIC PARTICLE MOTION IN TWO WAVES

In this section we discuss a simple dynamical system exhibiting both regular and stochastic motion. Both types of motion will be observed in Sec. IV for the more complicated dynamical system suggested by the beam-plasma problem. Here, we consider the one-dimensional motion of a particle in the presence of two waves. The first wave has a much greater amplitude than the second wave, which is treated as a perturbation. The unperturbed problem is described by the Hamiltonian

$$H_0(x,p) = \tfrac{1}{2}p^2 - \cos x \ , \tag{1}$$

where x and p are the position and momentum of the particle, and where we have chosen to work in a reference frame moving with the phase velocity of the first wave. In (1) we use units such that the mass of the particle and the wavenumber and amplitude of the first wave are unity. In Fig. 1(a) we show the potential energy $V(x) = -\cos x$. The Hamiltonian (1) describes many other physical systems, a nonlinear pendulum being the best-known example. Theoretical treatment of (1) is easiest in action-angle variables. These variables are defined in such a way that the unperturbed Hamiltonian depends on the action J but not on the angle ϕ: $H_0 = H_0(J)$. The relations between the variables x and p used in (1) and the variables J and ϕ are given in the Appendix. Physically, the action J represents the area (divided by 2π) bounded by a trajectory in the xp phase space. When J reaches $8/\pi \approx 2.55$, the particle trajectory coincides with the separatrix, which divides phase space into trapped and untrapped regions. In Fig. 1(b) we show the trajectory of a particle trapped in the trough of the first wave. The angle ϕ represents the phase of the bouncing motion in the trough.

The equations of motion derived from $H_0(J)$ are extremely simple

$$dJ/dt = -\partial H_0/\partial\phi = 0 \rightarrow J(t) = J(t=0) \ , \tag{2a}$$

$$d\phi/dt = \partial H_0/\partial J \equiv \omega_b(J) = \text{const} \ . \tag{2b}$$

The bounce frequency ω_b, defined in (2b), is unity for a deeply trapped particle ($J=0$) and decreases as J in-

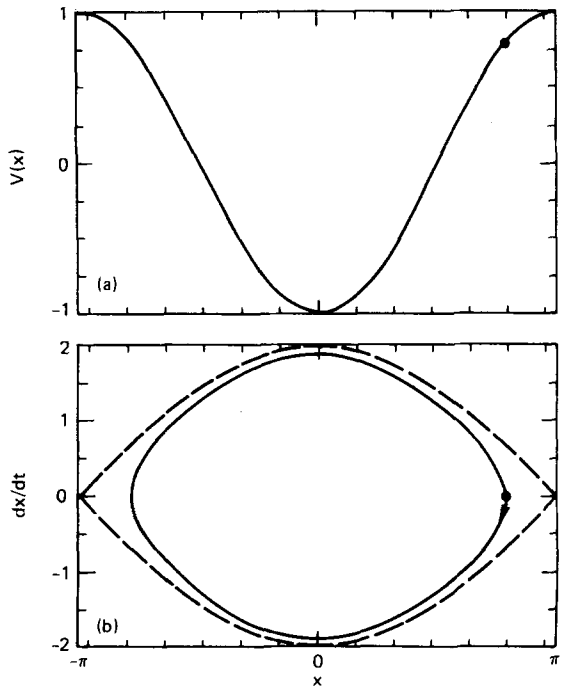

FIG. 1. Plots illustrating the dynamical system described by the Hamiltonian (1). (a) The potential energy well $V(x) = -\cos x$. (b) The phase plane of dx/dt vs x, showing the trajectory (solid line) of a particle with $H_0 = 0.8$. The dashed line is the separatrix ($H_0 = 1$).

creases. The formula for $\omega_b(J)$ is given in the Appendix.

We next study the effect on the particle motion of a second wave of amplitude ϵ, wavenumber k, and frequency Ω. The Hamiltonian becomes

$$H(x,p,t) = H_0(x,p) + H_1(x,t) , \tag{3a}$$

$$H_1 = -\epsilon\cos(kx - \Omega t) . \tag{3b}$$

In terms of the action-angle variables, the Hamiltonian appears as follows:

$$H(\phi, J, t) = H_0(J) + H_1(\phi, J, t) , \tag{4a}$$

$$H_1 = -\epsilon\sum_{n=-\infty}^{\infty} V_n(J,k)\cos(n\phi - \Omega t) . \tag{4b}$$

In (4b) the perturbation is expressed as a Fourier series in the angle ϕ. The Fourier coefficients

$$V_n(J,k) \equiv \frac{1}{2\pi}\int_{-\pi}^{\pi} d\phi[\cos kx(\phi, J) - n\phi] \tag{5}$$

can be written explicitly only in certain limiting cases. For our purposes, an adequate approximation, exact in the limit $J \to 0$, is

$$V_n(J,k) \approx J_n[k(2J)^{1/2}] , \tag{6}$$

where J_n denotes the Bessel function of the first kind. (See the Appendix for further information on the V_n.)

The second wave introduces into the motion an infinite number of resonances. These bounce resonances, as we call them, are apparent after a trivial analysis of (4). Since ϵ is treated as small, we neglect H_1 when calculating $d\phi/dt$ and use (2b) as an approximation. The phase of the nth term in (4b) is thus slowly varying in time if

$$n\, d\phi/dt \approx n\omega_b(J) \approx \Omega . \tag{7}$$

The particle is near the nth bounce resonance if its J satisfies (7).

For the bounce resonances, (7) gives the resonant values of the action J and, therefore, the separation between the resonances in action space. A width can be assigned to each bounce resonance; this width is analogous to the trapping width one calculates for an electron in the presence of a Langmuir wave. When resonance widths exceed separations, one says that resonances overlap. Overlap of resonances results in stochastic motion,[24] which has two important properties. First, a constant of the motion that exists when resonances do not overlap disappears when resonances begin to overlap. The loss of a constraint on the motion allows the particle to visit regions of phase space not otherwise accessible to it. Second, when motion is stochastic, two particles initially close to each other in phase space rapidly move apart. Therefore, a bunch of particles, such as occurs in the beam-plasma interaction, will disperse when motion is stochastic.

Overlap of bounce resonances has frequently been used[24-27] to show that motion near the separatrix is stochastic. However, a numerical study of particle motion in two waves[28] demonstrated that even with a modest ϵ ($= 0.2$), motion could be stochastic in a large region of phase space, not just near the separatrix where overlap of bounce resonances could be invoked. In Sec. IV we show that the wave which occurs in the nonlinear stage of beam-plasma interaction also causes stochastic motion in a large region of phase space.

On the other hand, regular motion is found to occur in an important region of phase space. For the parameters suggested by the problem of beam-plasma interaction, we can easily describe the regular motion analytically. The value of the frequency parameter is

$$\Omega = \omega_b(0) , \tag{8}$$

which implies that the $n = 1$ bounce resonance (7) should be important for deeply trapped particles (i.e., those with small J). Indeed, a fair approximation for the regular motion is obtained by neglecting all terms in (4b) except that for $n = 1$

$$H^{(1)}(\phi, J, t) = H_0(J) - \epsilon V_1(J,k)\cos(\phi - \Omega t) . \tag{9}$$

We reduce (9) to a problem with one degree of freedom by using a generating function[29]

$$F_2(\phi, J', t) = (\phi - \Omega t)J' , \tag{10}$$

which produces the canonical transformation

$$J' = \partial F_2/\partial\phi = J , \tag{11a}$$

$$\psi = \partial F_2/\partial J' = \phi - \Omega t , \tag{11b}$$

$$K^{(1)}(\psi, J) = H^{(1)} + \partial F_2/\partial t = H_0(J) - \Omega J - \epsilon V_1(J,k)\cos\psi . \tag{11c}$$

In the transformed Hamiltonian (11c), we have dropped the prime on J by virtue of (11a). The motion described by (11c) includes fixed points, defined by

$$d\psi/dt = \partial K^{(1)}/\partial J = 0 , \tag{12a}$$

and

$$dJ/dt = -\partial K^{(1)}/\partial\psi = -\epsilon V_1\sin\psi = 0 . \tag{12b}$$

The simultaneous satisfaction of Eqs. (12) requires

$$\psi = 0 \text{ or } \pi \ , \tag{13a}$$

and

$$\Omega - \omega_b(J) \pm \epsilon(\partial V_1/\partial J) = 0 \ . \tag{13b}$$

The plus sign in (13b) goes with the $\psi = 0$ solution of (13a), the minus sign with $\psi = \pi$. The $\psi = \pi$ solution turns out to be a *stable* fixed point, near which regular motion occurs. To our knowledge, no existing theory can predict the size or shape of the region of regular motion. We find this region by numerically calculating particle trajectories.

The value of J at which the stable fixed point occurs can be estimated using (6), (13b), and the small-J approximation

$$\omega_b(J) = \omega_b(0)\,(1 - J/8) + O(J^2) \tag{14}$$

derived in the Appendix. With our choice of units, $\omega_b(0) = 1$ and the J value at the stable fixed point is

$$J \approx 2(k\epsilon)^{2/3} \ . \tag{15}$$

We emphasize that the most stable motion occurs not for a particle at the bottom of the trough ($J = 0$), but for one with a certain amplitude of oscillation about the bottom.

The true particle motion derived from (4) differs from the motion described by (9) or equivalently, (11c). In particular, a true trajectory initially at the stable fixed point shows oscillations in J away from (15). We have been able to describe these oscillations by using the $n = 2$ and $n = -1$ terms of (4b).

In summary, in this section we have described the nature of particle motion in two waves for moderate amplitude ϵ, wavenumber $k \approx 1$, and frequency Ω given by (8). In the vicinity of the stable fixed point, the motion is regular and can be treated with the approximate Hamiltonian (9). Away from the stable fixed point the motion is stochastic, and only qualitative descriptions of the motion are available.

III. MODEL FOR AN OSCILLATING WAVE

In this section we describe our model for a wave with oscillating amplitude and phase (termed "an oscillating wave"). This model should give an adequate description for particle motion in the nonlinear stage of the Dimonte–Malmberg experiment and in some beam-plasma and launched-wave experiments.

We study particle motion in the potential

$$\Phi(x,t) = \bar{\Phi}(t)\cos[kx - \theta(t)] \ . \tag{16}$$

The amplitude oscillations are taken to be sinusoidal with frequency Ω,

$$\bar{\Phi}(t) = \Phi_0[1 + \epsilon\cos(\Omega t)] \ . \tag{17}$$

We shall discuss our choices for ϵ and Ω. The phase oscillations have components at two frequencies, Ω and 2Ω,

$$\theta(t) = \theta_0 \sin(\Omega t) - \theta_1 \sin(2\Omega t) \ . \tag{18}$$

(The parameters θ_0 and θ_1 are chosen later.) Note that we have removed the linear part (ωt) of the wave phase by working in a reference frame moving with the time-averaged phase velocity. Phase oscillations at twice the frequency of the amplitude oscillations were predicted by Morales and O'Neil[2] using a theory that was not self-consistent. The semi-simulations of O'Neil *et al.*[4] clearly showed that the phase oscillations have components at both Ω and 2Ω. The analytical "rotating-bar" model of Mynick and Kaufman,[30] which is self-consistent, provides physical insight into the origin of the components at Ω and 2Ω.

We feel that the self-consistent evolution of the wave amplitude and phase has been adequately established by semi-simulation and laboratory experiments. Our goal is to clarify the particle motion in this given wave. Understanding the particle motion, in principle, allows one to explain features of the self-consistent wave evolution without resort to semi-simulation methods.

In choosing values for the parameters ϵ, Ω, θ_0, and θ_1, we use information from Refs. 4 and 11. The universal solution of Ref. 4 gives a peak amplitude roughly 40% above the average amplitude, which is consistent with the experiment of Dimonte and Malmberg.[11] We thus choose

$$\epsilon = 0.4 \tag{19}$$

in Eq. (17). Reference 4 also shows that the frequency Ω of the amplitude modulation is very nearly given by

$$\Omega = \omega_b(0) \equiv k(e\Phi_0/m)^{1/2} \ , \tag{20}$$

where e and m are the magnitudes of the electron charge and mass. Physically, Eq. (20) follows from the fact that the amplitude oscillations are caused by the bouncing of electrons trapped near the bottom of the potential wells.

We choose

$$\theta_0 = 0.2 \ , \qquad \theta_1 = 0.1 \tag{21}$$

after analyzing the curve for $\Omega_r(\tau)$, the real part of the scaled and Doppler-shifted wave frequency, given in Fig. 2 of Ref. 4. This curve is related to our $d\theta/dt$ by

$$\frac{d\theta}{dt} = \frac{d\tau}{dt}\,\{\Omega_r[\tau = \tau_0 + (\mathrm{Re}\,\omega - ku_0)t] - \bar{\Omega}_r\} \ , \tag{22}$$

where τ is the scaled time variable,[4] τ_0 is the value of τ at the first maximum of the wave amplitude, $\bar{\Omega}_r$ is the value Ω_r averaged over times beyond τ_0, and u_0 is the initial beam velocity.

The forms for $\bar{\Phi}(t)$ and $\theta(t)$ resulting from these parameters are shown in Fig. 2.

Now, we show that the equations of particle motion in the potential (16) are quite similar to those studied in Sec. II. We neglect θ_1 in (18) and keep only terms up to first order in θ_0

$$\cos[kx - \theta(t)] \approx \cos(kx) + \theta_0 \sin(\Omega t)\sin(kx) \ . \tag{23}$$

We multiply (23) by (17) and neglect the product $\epsilon\theta_0$:

$$\begin{aligned}\Phi(x,t) &\approx \Phi_0[\cos(kx) + \epsilon\cos(\Omega t)\cos(kx) + \theta_0 \sin(\Omega t)\sin(kx)] \\ &= \Phi_0[\cos(kx) + \epsilon_1\cos(kx - \Omega t) + \epsilon_2\cos(kx + \Omega t)] \ ,\end{aligned} \tag{24}$$

where

$$\epsilon_1 \equiv \tfrac{1}{2}(\epsilon + \theta_0) = 0.3 \ , \qquad \epsilon_2 \equiv \tfrac{1}{2}(\epsilon - \theta_0) = 0.1 \ . \tag{25}$$

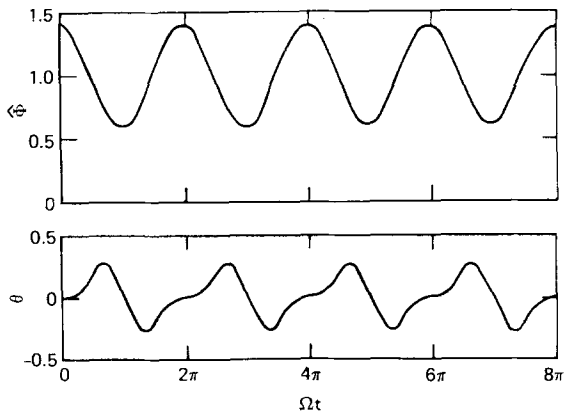

FIG. 2. The amplitude $\bar{\Phi}$ and phase θ of an oscillating wave given by (17) and (18) with parameters (19) and (21).

With a choice of units such that

$$m = k = e\Phi_0 = 1 , \tag{26}$$

the Hamiltonian describing motion in (24) has exactly the form (3a), with H_0 given by (1) and

$$H_1 = -\epsilon_1 \cos(x - \Omega t) - \epsilon_2 \cos(x + \Omega t) . \tag{27}$$

In terms of the action-angle variables introduced in Sec. II, (27) can be written

$$H_1 = -\sum_{n=-\infty}^{\infty} U_n(J) \cos(n\phi - \Omega t) , \tag{28}$$

where

$$U_n(J) = \epsilon_1 V_n(J, 1) + \epsilon_2 V_n(J, -1) , \tag{29a}$$

$$U_n(J) = [\epsilon_1 + (-1)^n \epsilon_2] V_n(J, 1) . \tag{29b}$$

For (29b) we used

$$V_n(J, -k) = (-1)^n V_n(J, k) , \tag{30}$$

which is easily proved using (5) and $x(\phi - \pi) = -x(\phi)$. The similarity of (4b) and (28) indicates that our understanding of particle motion in two waves (Sec. II) can be applied to motion in a wave with oscillating amplitude and phase. The approximations we have made in deriving (24) [and thus (27) and (28)] do not invalidate this conclusion, as shown by numerical results, which we present later.

In laboratory experiments involving a large-amplitude wave, the frequency is fixed and the wave amplitude and phase oscillate in space. Instead of (16), particles feel the potential

$$\Phi(x', t) = \bar{\Phi}(x') \cos[kx' - \omega t - \theta(x')] , \tag{31}$$

where x' is measured in the laboratory frame of reference and ω is the wave frequency. We introduce the coordinate

$$x = x' - (\omega/k)t , \tag{32}$$

which measures distance in the wave frame of reference, and we assume $\bar{\Phi}$ and θ have forms analogous to (17) and (18):

$$\bar{\Phi}(x') = \Phi_0[1 + \epsilon \cos(k_b x')] , \tag{33}$$

$$\theta(x') = \theta_0 \sin(k_b x') - \theta_1 \sin(2k_b x') , \tag{34}$$

where one period of the amplitude oscillation occurs in a distance $2\pi/k_b$. Again making the approximations which led to (24), we find the potential in the wave frame to be given by

$$\Phi(x, t) \approx \Phi_0[\cos(kx) + \epsilon_1 \cos(kx - k_b x') + \epsilon_2 \cos(kx + k_b x')] . \tag{35}$$

From (32) we write

$$kx \pm k_b x' = (k \pm k_b)x \pm (k_b \omega/k)t \tag{36}$$

and define

$$k_\pm \equiv k \pm k_b , \qquad \Omega \equiv k_b \omega/k . \tag{37}$$

The potential (35) thus has the final form

$$\Phi(x, t) \approx \Phi_0[\cos(kx) + \epsilon_1 \cos(k_- x - \Omega t) + \epsilon_2 \cos(k_+ x + \Omega t)] . \tag{38}$$

We see that the spatial (boundary-value) problem leads to a potential (38) differing in a simple way from the potential (24) occurring in the temporal (initial-value) problem. The perturbation can still be written in the form (28), but

$$U_n(J) = \epsilon_1 V_n(J, k_-/k) + \epsilon_2 V_n(J, -k_+/k) . \tag{39}$$

In the Dimonte–Malmberg experiment, $k_b/k \approx 0.2$, and detailed results derived using (39) would differ somewhat from the results for a corresponding temporal problem, which would use (29).

IV. PARTICLE MOTION IN AN OSCILLATING WAVE

We now describe the particle trajectory calculations we have carried out. The oscillating wave has the potential given by Eqs. (16)–(21), which is appropriate to temporal (initial-value) problems. For the results presented here we have not made the approximations leading to (24); the results obtained with Eq. (24) are quite similar, however, to those obtained with Eq. (16). We have studied (16) rather than (31) because the former is somewhat simpler. It is clear from the results of Sec. III that qualitatively similar trajectories occur for temporal and spatial problems.

The Hamiltonian

$$H(x, p, t) = p^2/2m - e\Phi(x, t) \tag{40}$$

gives the equations of motion

$$dx/dt = \partial H/\partial p = p/m , \tag{41a}$$

$$dp/dt = -\partial H/\partial x = e\,\partial\Phi/\partial x . \tag{41b}$$

With the units specified by (26) and the specific model of Eqs. (16)–(18), the equations of motion (41) take the explicit form

$$dx/dt = p , \tag{42a}$$

$$dp/dt = -[1 + \epsilon \cos(\Omega t)] \sin[x - \theta(t)] . \tag{42b}$$

Equations (42) were integrated numerically using an accurate scheme, which is discussed in Ref. 31.

Previous workers have displayed particle trajectories on the xp plane by using the curve traced by a particle during its motion in the plane. Instead, we display the calculated trajectories using a stroboscopic plot. This type of plot is constructed by recording a point on the xp plane whenever $\Omega t/2\pi$ is an integer. Figure 3 shows

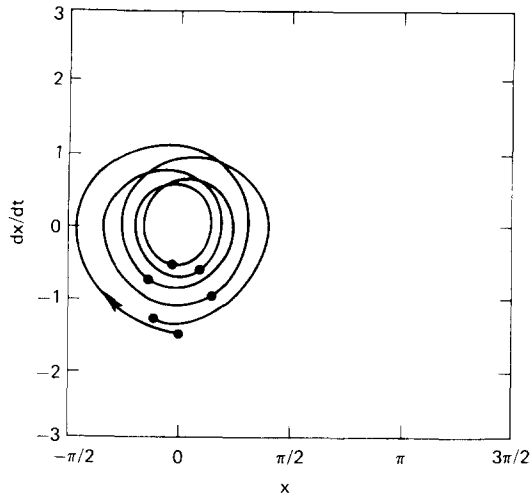

FIG. 3. Comparison of a plot of a complete trajectory (the curve) with the points used for a stroboscopic plot. The trajectory shown here is one of five used to produce Fig. 4.

how a stroboscopic plot differs from the type of plot used previously. The curve was traced by a particle during its motion; the points constitute a stroboscopic plot. Stroboscopic plots allow us to distinguish at a glance between regular and stochastic motion. Stochastic motion is characterized by a particle trajectory that wanders throughout a three-dimensional subspace of xpt space, where x and Ωt are modulo 2π. On a stroboscopic plot such a trajectory appears as a set of scattered points. On the other hand, the existence of a constant of the motion constrains a regular trajectory to a two-dimensional subspace of xpt space. On a stroboscopic plot a regular trajectory appears as a set of points that seem to lie on one or more curves. The curves on our stroboscopic plots are not trajectories but merely aids for the eye in connecting points resulting from a single trajectory.

The two classes of motion, regular and stochastic, are shown in Fig. 4. To produce Fig. 4, we used five

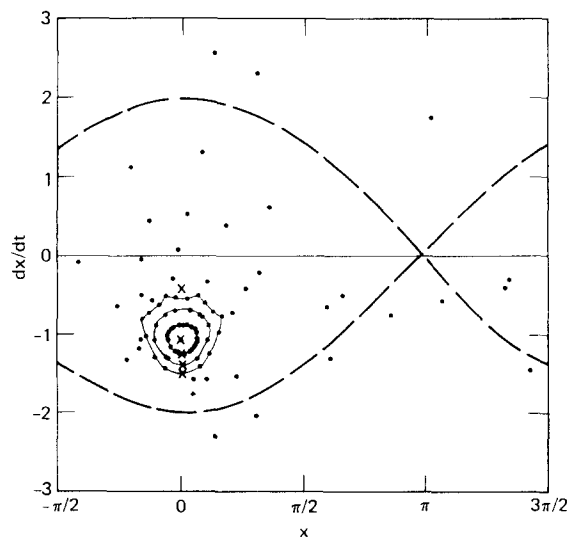

FIG. 4. Stroboscopic plot of five particle trajectories in the potential given by Eqs. (16)–(21).

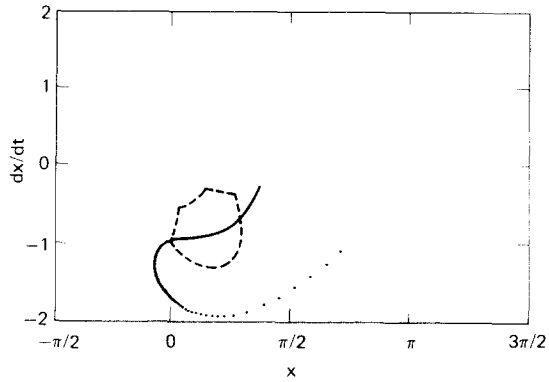

FIG. 5. Comparison of the locations in phase space of the regular region and of the beam particles used in Ref. 4.

initial values of x and p, indicated by crosses. Four of these initial conditions lead to regular trajectories, while one leads to a stochastic trajectory. One of the regular trajectories is very close to the stable-fixed-point trajectory. Because of the simple form of (29b) we can apply (15), after replacing $k\epsilon$ by $\epsilon_1 - \epsilon_2 = 0.2$, to find $J \approx 0.68$ as the predicted action value at the stable-fixed point. The calculated trajectories suggest that the fixed point is located at $J \approx 0.59$, which is satisfactory agreement. The dashed curve in Fig. 4 is the separatrix, defined by $H_0 = 1$. In a wave without an oscillating amplitude or phase ($\epsilon = \theta_0 = \theta_1 = 0$), a particle that is inside the separatrix at $t = 0$ remains trapped forever. In an oscillating wave, a particle can cross the separatrix and move from one potential well to another.

The regular trajectories in Fig. 4 map out a region in the xp plane that we call the "regular region." The existence of this region and its location near the stable fixed point imply a phase-locking effect. This effect replaces the phase-mixing process, which is usually invoked to explain decay of amplitude and phase oscillations. In a nonoscillating wave, particles trapped at different depths in the potential well bounce with different frequencies, i.e., $\omega_b = \omega_b(J)$. The phases ϕ of different particles gradually lose any coherence they had initially. In an oscillating wave, on the other hand, the phases of particles in the regular region all increase at a time-averaged rate Ω. Stating the same fact differently, we say that the variable $\psi = \phi - \Omega t$ never differs much from π, or that the particles return to the same region of phase space whenever $\Omega t/2\pi$ is an integer. The phases ϕ_i of N regularly moving particles ($i = 1, 2, \ldots, N$) satisfy

$$|\phi_i - \phi_j| \ll 2\pi \tag{43}$$

for all pairs of i and j and for all time.

The regular region occupies only a small fraction of the trapped part of phase space. The initial evolution of the beam-plasma instability tends to bunch most of the beam particles into a small region of phase space. At the time of saturation (our $t = 0$), are the beam particles located in the regular region we have found? Although it may seem improbable, the answer is apparently yes. In Fig. 5 we compare the location in phase space of the regular region and of the beam particles. For the beam particles we use the results in Ref. 4,

Fig. 3, for $\tau = 6.0$. This value of τ is just before saturation ($\tau_0 \approx 6.4$) and corresponds to our $\Omega t \approx -0.5$. Plotting points of the outermost regular trajectory from our Fig. 4 when $\Omega t = -0.5 + 2\pi N$ ($N = 0, 1, 2, \ldots$), yields an approximate boundary of the regular region. This boundary is shown by the dashed curve in Fig. 5. In superposing the beam particles from Ref. 4 with our regular region we have taken into account differences in the variables used by them and by us. Their unit of time is longer than ours by a factor of roughly 1.2 (observe the periods in Fig. 2 of Ref. 4), resulting in different units for velocity. Their spatial variable ξ and our x are measured in different reference frames ($d\xi/dt = -0.68$ corresponds to our $dx/dt = 0$). Also, the trough of the wave, which is moving in their reference frame, must be located at $\tau = 6.0$ (we find the trough to be at $\xi = -0.15$). Information for these determinations has been derived from Fig. 2 of Ref. 4. The resulting superposition in our Fig. 5 shows that many of the beam particles lie in our regular region. Beam particles outside, but close to, the regular region often remain near the regular region for many periods $2\pi/\Omega$, according to our trajectory calculations. In a finite-time experiment the regular region is therefore somewhat larger, effectively, than indicated in Fig. 5.

V. ADDITION OF A TEST WAVE

In the previous sections we have developed an understanding of the persistence of amplitude and phase oscillations of a single wave. In experiments this single wave (here called the main wave) dominates the electric-field spectrum for a certain (spatial) interval after saturation. In the Dimonte–Malmberg experiment, this interval could exceed the entire length of the experiment. Alternatively, the experimenters could observe development of a broad spectrum by launching a smaller-amplitude wave (called the test wave) in addition to the main wave. The launched test wave can be viewed as a model for any wave, other than the main wave, that grows because of the linear beam-plasma instability or any of the sideband instability mechanisms mentioned in Sec. I.

In this section we study the effect of a test wave on the regular motion observed in Sec. IV. We find that a test wave can prevent the regular, phase-locked motion essential for persistent amplitude oscillations. As a test wave grows in an experiment, its amplitude will become large enough at some point to destroy the amplitude oscillations of the main wave.

We compute particle trajectories using (40), but now the potential of the main wave is augmented by that of the test wave

$$\Phi(x,t) = \Phi(t)\cos[kx - \theta(t)] + \epsilon_t \Phi_0 \cos(k_t x - \Omega_t t + \eta) . \tag{44}$$

The parameters ϵ_t, k_t, Ω_t, and η are held fixed in all runs except for a few in which ϵ_t varies in time. Various values for the test-wave amplitude ϵ_t, ranging up to 0.3, are used. The values for the test-wave wavenumber k_t and frequency Ω_t correspond to those used for Fig. 3 of Ref. 11. From the frequencies of the main and test waves given there and the measured dispersion relation[12] we take

$$k_t = (1.3)k = 1.3 . \tag{45}$$

Remembering that we are working in the frame of the main wave, we choose

$$\Omega_t = \omega_t - k_t\omega/k \approx -\tfrac{2}{3}\Omega = -\tfrac{2}{3} , \tag{46}$$

where ω_t is the test-wave frequency as measured in the laboratory. The parameter η is the relative phase between the main and test waves at $t = 0$ as felt by a particle at $x = 0$. Because the test wave has a different wavenumber than the main wave, a different value of η is appropriate for a particle located at $kx = 2\pi$ at $t = 0$. In a spatial (boundary-value) problem, different values of η are appropriate for particles that were injected into the plasma (or traveling-wave tube) at different times and which therefore became trapped in different troughs of the main wave. All of the results presented here have

$$\eta = 0 . \tag{47}$$

Runs with other values of η are similar qualitatively, but can be quite different quantitatively.

In Fig. 6 we show stroboscopic plots of particle trajectories in the potential given by Eqs. (44)–(47). For Fig. 6(a) ϵ_t equals 0.1, which is roughly the value observed by Dimonte and Malmberg at the first maximum of the main-wave power (our $t = 0$). For Fig. 6(b) ϵ_t equals 0.2, which is roughly the value they observed at the first minimum (our $t = \pi/\Omega$). As the value of ϵ_t is increased, we see that the regular region is displaced to more negative values of dx/dt. However, the size of the regular region seems to be changed only slightly by a change in ϵ_t, although the regular regions in Fig. 6 are smaller than that in Fig. 4 ($\epsilon_t = 0$). Detailed study of regular trajectories like those plotted in Fig. 6 reveals that the particle undergoes large excursions in H_0 (or equivalently, in J). The amplitudes of the excursions increase as ϵ_t increases. Also, the location of the regular region varies a great deal if η is changed, the variation increasing with increasing ϵ_t.

These results suggest the following mechanism for the destruction of amplitude oscillations in the Dimonte–Malmberg experiment. At the point of wave-growth saturation, the particles are distributed in phase space roughly as calculated by O'Neil *et al.*[4] As shown in Sec. IV, they are thus located in or near the regular region found for $\epsilon_t = 0$. The test wave grows rapidly, causing a displacement of the regular region away from the part of phase space where the particles are. The particles thus move stochastically; no phase locking occurs and the distribution of beam particles relaxes to a less coherent state. In this state the momentum and energy of the particles are more nearly constant, giving smaller oscillations in the wave power.

This scenario would be invalid if particle trajectories were displaced in the same way that the regular region is displaced. The rapid change of ϵ_t argues against such a displacement of particle trajectories, and we have conclusively ruled out this displacement with the following test. We allowed ϵ_t to vary in time according to

$$\epsilon_t(t) = \begin{cases} 0.1 + (\Omega t/\pi)0.1 , & 0 < \Omega t < 2\pi \\ 0.3 , & \Omega t > 2\pi . \end{cases} \tag{48}$$

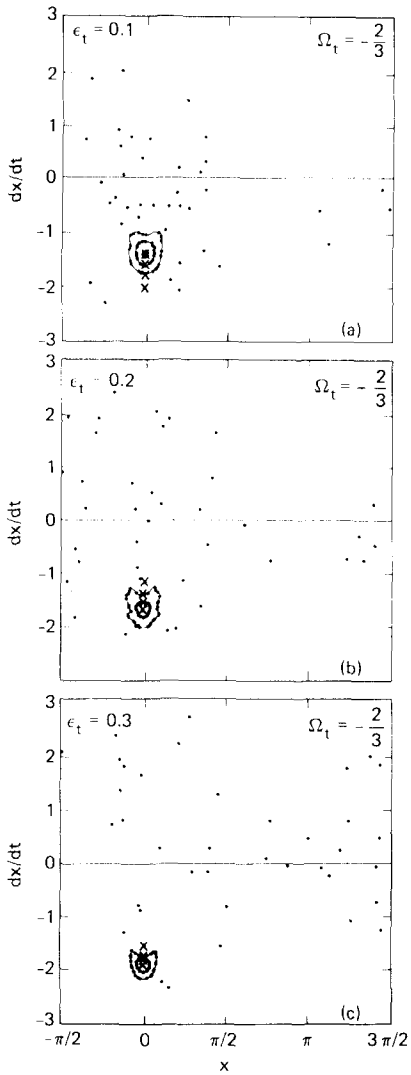

FIG. 6. Stroboscopic plots of particle trajectories in the presence of a test wave of frequency $\Omega_t = -2/3$, showing displacement of the regular region as the test-wave amplitude ϵ_t is increased. Points are plotted whenever $\Omega t/6\pi$ is an integer.

We calculated several representative trajectories whose initial values of x and dx/dt would have led to regular trajectories if ϵ_t were fixed at 0.1; the trajectories are stochastic when ϵ_t is given by (48).

Instead of being displaced, the regular region can completely disappear in the presence of a test wave. We illustrate this result in Fig. 7 for the potential specified by Eqs. (44), (45), (47), and

$$\Omega_t = 1.5 \,. \tag{49}$$

For $\epsilon_t = 0.05$ Fig. 7 gives a much smaller regular region than for $\epsilon_t = 0$ (Fig. 4). For $\epsilon_t = 0.1$ in Fig. 7 the regular region is even smaller, and for somewhat higher values of ϵ_t no regular trajectories at all can be found. We conclude that a strong enough test wave with frequency (49) destroys the phase-locking mechanisms and therefore the persistent amplitude oscillations.

VI. CONCLUSIONS

We have studied the motion of particles in electric fields that model the fields found in launched-wave or beam-plasma experiments. The single large-amplitude wave observed in these experiments can exhibit persistent amplitude oscillations because of a phase-locking effect. This effect replaces the well-known phase-mixing mechanism for decay of the amplitude oscillations. The phase-locking effect occurs in a certain part of phase space called the regular region. In the beam-plasma problem, this region is small, yet most beam particles are located in or near the region. The addition of a test wave of moderate amplitude causes displacement or outright disappearance of the regular region, which leads to dispersal of the bunched beam particles responsible for the amplitude oscillations.

ACKNOWLEDGMENTS

After we submitted this paper, Dr. R. N. Franklin brought to our attention later work[32] by his group that

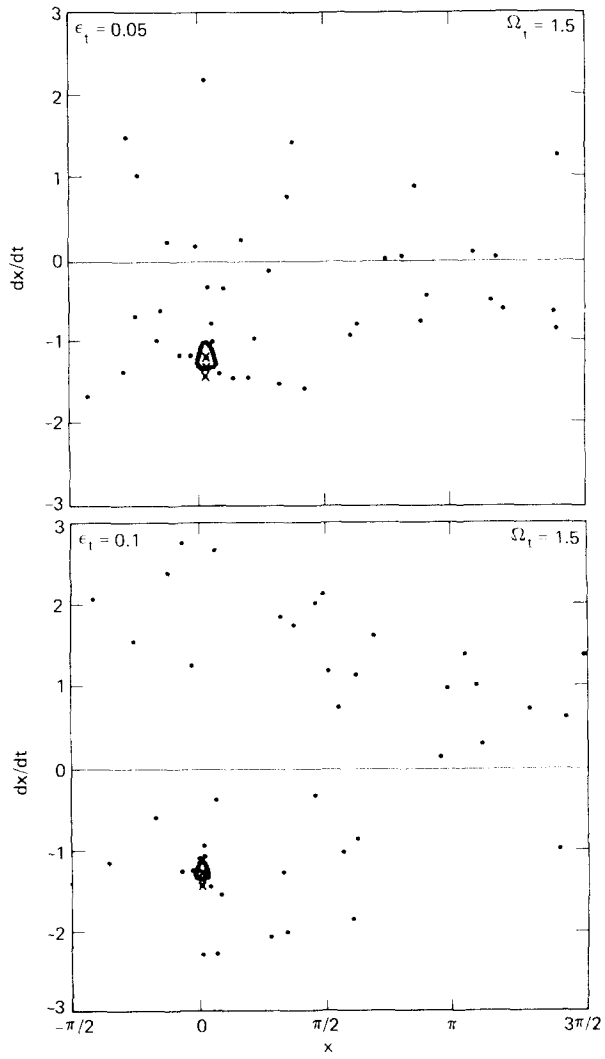

FIG. 7. Stroboscopic plots of particle trajectories in the presence of a test wave of frequency $\Omega_t = 1.5$, showing disappearance of the regular region as ϵ_t is increased. Points are plotted whenever $\Omega t/4\pi$ is an integer.

agrees with our belief in the quasi-linear mechanism of sideband growth.

We thank Guy Dimonte and John Malmberg for discussing their experiment with us on several occasions. Conversations with Allan Kaufman have also been very helpful.

This work was performed under the auspices of the U. S. Department of Energy by the Lawrence Livermore Laboratory, under contract number W-7405-Eng-48, and the Lawrence Berkeley Laboratory.

APPENDIX

Here, we give formulae arising in the transformation of

$$H_0 = \tfrac{1}{2}p^2 - \cos x \tag{A1}$$

to action-angle variables. The results are well known, but our approach might be instructive.

We introduce

$$y = \tfrac{1}{2}x \tag{A2}$$

and

$$\kappa^2 = \tfrac{1}{2}(1 + H_0) \tag{A3}$$

and note that

$$p = dx/dt \ . \tag{A4}$$

We can then write (A1) as

$$\kappa^2 = (dy/dt)^2 + \sin^2 y \ . \tag{A5}$$

A deeply trapped particle has $H_0 = -1$ and thus $\kappa = 0$; a particle on the separatrix has $H_0 = 1$ and $\kappa = 1$. The motion described by (A1) is given by functions sn, cn, and dn, which are defined by

$$\sin y = \kappa\,\mathrm{sn}(t - t_0) \ , \tag{A6a}$$

$$dy/dt = \kappa\,\mathrm{cn}(t - t_0) \ , \tag{A6b}$$

$$\cos y = \mathrm{dn}(t - t_0) \ . \tag{A6c}$$

We now show that these functions obey the relations that determine the Jacobian elliptic functions with the same names. [33] Differentiating (A6a) and using (A6b, c), we find

$$d[\mathrm{sn}(t - t_0)]/dt = \mathrm{cn}(t - t_0)\,\mathrm{dn}(t - t_0) \ . \tag{A7a}$$

Equations (A5) and (A6a, b) yield

$$\mathrm{cn}^2(t - t_0) + \mathrm{sn}^2(t - t_0) = 1 \ . \tag{A7b}$$

Combining (A6a) and (A6c) gives

$$\mathrm{dn}^2(t - t_0) + \kappa^2\,\mathrm{sn}^2(t - t_0) = 1 \ . \tag{A7c}$$

Together with $\mathrm{sn}0 = 0$, Eqs. (A7) are the determining relations used by Whittaker and Watson. [33]

We introduce the angle variable ϕ, which satisfies (2b):

$$\phi = \phi_0 + \omega_b(J)t \ . \tag{A8}$$

We choose t_0 such that

$$\phi = \omega_b(J)\,(t - t_0) \tag{A9}$$

and note the relation between ϕ and x that follows from (A2), (A6a), and (A9):

$$x(\phi, J) = 2\sin^{-1}[\kappa\,\mathrm{sn}(\phi/\omega_b)] \ . \tag{A10}$$

We want a 2π change in ϕ to correspond to one period, and sn has periodicity $4K(\kappa)$ where $K(\kappa)$ is the complete elliptic integral of the first kind with modulus κ. The bounce frequency is thus given as a function of $J = J(\kappa)$ by

$$\omega_b(J) = \pi/2K(\kappa) \ . \tag{A11}$$

The relation between J and κ follows from (A11) and from

$$\omega_b = \frac{dH_0}{dJ} = \frac{dH_0}{d\kappa}\,\frac{d\kappa}{dJ} = 4\kappa\,\frac{d\kappa}{dJ} \tag{A12}$$

by integration:

$$J = (8/\pi)\int \kappa K(\kappa)\,d\kappa \tag{A13a}$$

$$J = (8/\pi)[E(\kappa) - (1 - \kappa^2)K(\kappa)] \ , \tag{A13b}$$

where $E(\kappa)$ is the complete elliptic integral of the second kind. For (A13b) we use a formula found, for example, in Gradshteyn and Ryzhik. [34] In the limit $\kappa \to 0$ the motion becomes simple harmonic and

$$\mathrm{sn}(t - t_0) \to \sin\phi \ , \tag{A14a}$$

$$\mathrm{cn}(t - t_0) \to \cos\phi \ , \tag{A14b}$$

$$\mathrm{dn}(t - t_0) \to 1 \ , \tag{A14c}$$

$$x \to 2\kappa\sin\phi \ , \tag{A14d}$$

$$J \to 2\kappa^2 = 1 + H_0 \ . \tag{A14e}$$

In (14) in Sec. II we use a result containing a correction term of higher order in κ^2. From (A11) and the series[34] for $K(\kappa)$ in powers of κ^2, we find

$$\omega_b(J) \approx \left(1 + \frac{\kappa^2}{4}\right)^{-1} \approx 1 - \frac{J}{8} \ . \tag{A15}$$

Next, we find explicit forms for the Fourier coefficients $V_n(J, k)$ defined in Eq. (5). In the limit $\kappa \to 0$ we can use (A14d, e) and the Bessel function identity

$$\cos(2k\kappa\sin\phi) = \sum_{n=-\infty}^{\infty} J_n(2k\kappa)\cos(n\phi) \tag{A16}$$

to derive (6) for arbitrary k.

For arbitrary κ in the interval $0 \le \kappa < 1$, we can calculate $V_n(J, k)$ for half-integer values of k. Since $x(-\phi, J) = -x(\phi, J)$, Eq. (5) can be rewritten as

$$V_n(J, k) = \frac{1}{2\pi}\int_{-\pi}^{\pi} d\phi\,\exp\{i[kx(\phi, J) - n\phi]\} \ . \tag{A17}$$

From (A6a, c) we have

$$\exp(ikx) = \exp(i2ky) = [\mathrm{dn}(\phi/\omega_b) + i\kappa\,\mathrm{sn}(\phi/\omega_b)]^{2k} \ . \tag{A18}$$

For $k = \frac{1}{2}$, the V_n are easily found by looking up the Fourier decomposition of dn and sn. [34] The case of most interest for this paper is $k = 1$, which we treat by contour integration.

We change variables to $u = \phi/\omega_b$ and use (A17), (A18), and the periodicity of the integrand to write

$$V_n = \frac{1}{4K}\int_0^{4K} du(\mathrm{dn}u + i\kappa\,\mathrm{sn}u)^2\exp(-in\pi u/2K) \ . \tag{A19}$$

For the integration contour, shown in Fig. 8, we choose

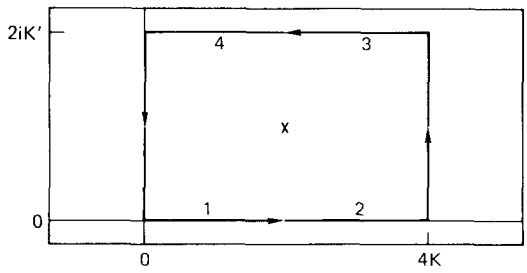

FIG. 8. The contour in the complex u plane used in evaluating (A19). The pole is shown by the cross.

the rectangle with vertices 0, $4K$, $4K+2iK'$, and $2iK'$, where $K' \equiv K[(1-\kappa^2)^{1/2}]$. The periodicity properties of dn and sn yield two results. First, the contributions to the contour integral of the vertical sides of the rectangle cancel. Second, the contribution of the segment marked 3 equals that of segment 1 times

$$-\exp[-in\pi(2K+2iK')/2K] = -(-q)^{-n} , \tag{A20}$$

where the nome

$$q \equiv \exp(-\pi K'/K) . \tag{A21}$$

The same result holds for segments 4 and 2, allowing us to write

$$V_n = \{4K[1-(-q)^{-n}]\}^{-1} 2\pi i \, \Sigma R , \tag{A22}$$

where R denotes the residue at a pole. Within the integration contour, the integrand in (A19) has only one singularity (a double pole) at $u = 2K + iK' \equiv u_0$. Defining $v \equiv u - u_0$ and using the expansions of dn and sn about $u = iK'$ given in Ref. 33, Sec. 22.341, we find

$$(\mathrm{dn}u + i\kappa \,\mathrm{sn}u)^2 \exp(-in\pi u/2K)$$
$$\approx -(-q^{1/2})^{-n}[4v^{-2} + O(v^0)] \exp(-in\pi v/2K) . \tag{A23}$$

Thus,

$$R = (2in\pi/K)(-q^{1/2})^{-n} , \tag{A24}$$

and from (A22)

$$V_n(J,1) = \frac{(\pi/K)^2 n q^{n/2}}{1-(-q)^n} . \tag{A25}$$

Equation (A10) is valid for all integers $n \neq 0$. For $n = 0$,

$$V_0(J,1) = 2E/K - 1 . \tag{A26}$$

[1]T. M. O'Neil, Phys. Fluids **8**, 2255 (1965).
[2]G. J. Morales and T. M. O'Neil, Phys. Rev. Lett. **28**, 417 (1972).
[3]P. J. Vidmar, J. H. Malmberg, and T. P. Starke, Phys. Fluids **19**, 32 (1976).
[4]T. M. O'Neil, J. H. Winfrey, and J. H. Malmberg, Phys. Fluids **14**, 1204 (1971).
[5]I. H. Oei and D. G. Swanson, Phys. Fluids **15**, 2218 (1972).
[6]Y. Matsuda and F. W. Crawford, Phys. Fluids **18**, 1336 (1975).
[7]I. H. Oei and D. G. Swanson, Phys. Fluids **17**, 856 (1974).
[8]R. Sugihara and T. Kamimura, J. Phys. Soc. Jpn. **33**, 206 (1972).
[9]S.-T. Tsai, J. Plasma Phys. **11**, 213 (1974).
[10]N. G. Matsiborko, I. N. Onishchenko, Ya. B. Fainberg, V. D. Shapiro, and V. I. Shevchenko, Zh. Eksp. Teor. Fiz. **63**, 874 (1972) [Sov. Phys.-JETP **36**, 460 (1973)].
[11]G. Dimonte and J. H. Malmberg, Phys. Rev. Lett. **38**, 401 (1977).
[12]G. Dimonte, Ph.D. thesis, University of California, San Diego (1977); G. Dimonte and J. H. Malmberg, Phys. Fluids **21**, 1188 (1978).
[13]C. B. Wharton, J. H. Malmberg, and T. M. O'Neil, Phys. Fluids **11**, 1761 (1968).
[14]G. J. Morales and J. H. Malmberg, Phys. Fluids **17**, 609 (1974).
[15]N. I. Budko, V. I. Karpman, and D. R. Shklyar, Zh. Eksp. Teor. Fiz. **61**, 1463 (1971) [Sov. Phys.-JETP **34**, 778 (1972)].
[16]A. L. Brinca, J. Plasma Phys. **7**, 385 (1972).
[17]M. N. Bussac, I. Mendonca, R. Pellat, and A. Roux, Phys. Rev. Lett. **33**, 349 (1974).
[18]G. Van Hoven and G. Jahns, Phys. Fluids **18**, 80 (1975).
[19]T. P. Starke and J. H. Malmberg, Phys. Rev. Lett. **37**, 505 (1976).
[20]N. Sato, G. Popa, E. Mark, R. Schrittwieser, and E. Mravlag, Phys. Rev. Lett. **37**, 1684 (1976).
[21]W. L. Kruer, J. M. Dawson, and R. N. Sudan, Phys. Rev. Lett. **23**, 838 (1969).
[22]R. N. Franklin, S. M. Hamberger, G. Lampis, and G. J. Smith, Proc. R. Soc. London A **347**, 1 (1975).
[23]G. Jahns and G. Van Hoven, Phys. Fluids **18**, 214 (1975).
[24]G. M. Zaslavskii and B. V. Chirikov, Usp. Fiz. Nauk **105**, 3 (1971) [Sov. Phys.-Usp. **14**, 549 (1972)]; J. Ford, in *Lectures in Statistical Physics*, edited by W. C. Schieve (Springer-Verlag, New York, 1974), Vol. 28, p. 204.
[25]M. N. Rosenbluth, R. Z. Sagdeev, J. B. Taylor, and G. M. Zaslavskii, Nucl. Fusion **6**, 297 (1966); N. N. Filonenko, R. Z. Sagdeev, and G. M. Zaslavskii, Nucl. Fusion **7**, 253 (1967).
[26]A. B. Rechester and T. H. Stix, Phys. Rev. Lett. **36**, 587 (1976).
[27]G. R. Smith, Phys. Rev. Lett. **38**, 970 (1977).
[28]G. R. Smith, in *Proceedings of the International Conference on Stochastic Behavior in Classical and Quantum Hamiltonian Systems*, Como, Italy (1977) (to be published).
[29]H. Goldstein, *Classical Mechanics* (Addison-Wesley, Reading, Mass., 1965), Chap. 8.
[30]H. E. Mynick and A. N. Kaufman, Phys. Fluids **21**, 653 (1978).
[31]G. R. Smith, Ph.D. thesis, University of California, Berkeley (1977).
[32]R. N. Franklin, R. R. MacKinlay, P. D. Edgley, and D. N. Wall, Proc. R. Soc. London A **360**, 229 (1978).
[33]E. T. Whittaker and G. N. Watson, *A Course of Modern Analysis* (Cambridge University Press, Cambridge, 1958), 4th ed., Chap. XXII.
[34]I. S. Gradshteyn and I. M. Ryzhik, *Table of Integrals, Series, and Products* (Academic, New York, 1965), Sec. 8.1.